Editors' Suggestion

Observation of Momentum Space Josephson Effects in Weakly Coupled Bose-Einstein Condensates

Annesh Mukhopadhyay,[1,*] Xi-Wang Luo,[2,3,4,*] Colby Schimelfenig,[1] M. K. H. Ome,[1] Sean Mossman,[1,5] Chuanwei Zhang,[6,7,†] and Peter Engels[1,‡]

[1]Department of Physics and Astronomy, Washington State University, Pullman, Washington 99164-2814, USA
[2]CAS Key Laboratory of Quantum Information, University of Science and Technology of China, Hefei, Anhui 230026, China
[3]Synergetic Innovation Center of Quantum Information and Quantum Physics, University of Science and Technology of China, Hefei, Anhui 230026, China
[4]Hefei National Laboratory, University of Science and Technology of China, Hefei 230088, China
[5]Department of Physics and Biophysics, University of San Diego, San Diego, California 92110, USA
[6]Department of Physics, The University of Texas at Dallas, Richardson, Texas 75080-3021, USA
[7]Department of Physics, Washington University in St. Louis, St. Louis, Missouri 63130, USA

(Received 13 November 2023; revised 13 April 2024; accepted 15 May 2024; published 7 June 2024)

The momentum space Josephson effect describes the supercurrent flow between weakly coupled Bose-Einstein condensates (BECs) at two discrete momentum states. Here, we experimentally observe this exotic phenomenon using a BEC with Raman-induced spin-orbit coupling, where the tunneling between two local band minima is implemented by the momentum kick of an additional optical lattice. A sudden quench of the Raman detuning induces coherent spin-momentum oscillations of the BEC, which is analogous to the ac Josephson effect. We observe both plasma and regular Josephson oscillations in different parameter regimes. The experimental results agree well with the theoretical model and numerical simulation and showcase the important role of nonlinear interactions. We also show that the measurement of the Josephson plasma frequency gives the Bogoliubov zero quasimomentum gap, which determines the mass of the corresponding pseudo-Goldstone mode, a long-sought phenomenon in particle physics. The observation of momentum space Josephson physics offers an exciting platform for quantum simulation and sensing utilizing momentum states as a synthetic degree.

DOI: 10.1103/PhysRevLett.132.233403

Introduction.—The Josephson effect describes supercurrents flowing between two reservoirs with a weak tunneling link (e.g., flow through a thin insulating barrier) [1,2]. Josephson effects have experimentally been observed in many platforms, ranging from solid state superconductors [3] to superfluid helium [4–8], exciton polaritons [9], and ultracold atomic gases [10–26]. Important applications of Josephson effects include superconducting quantum interference devices [27,28], superconducting qubits [29–32], and precision measurements [27].

In recent years, momentum states of ultracold bosons have emerged as a new synthetic degree of freedom for quantum matter and simulation. In this context, the Josephson effect in momentum space has been theoretically predicted for Bose-Einstein condensates (BECs) located at two momentum states with a weak coupling induced by momentum kicks of laser beams [33]. Such momentum space tunneling has been implemented in experiments using a Bragg transition for a single-component BEC [34,35] or an optical lattice in a spin-orbit coupled BEC [36]. Despite significant experimental progress in the observation of various forms of quantum dynamics in momentum space lattices (e.g., macroscopic quantum self-trapping or phase-driven nonlinear dynamics [34,35]), the momentum space Josephson oscillation has not been observed in experiments due to the challenge of realizing a coherent ground state BEC occupying two momentum states with a long lifetime.

In this Letter, we show experimental evidence for the momentum space Josephson effect in a spin-orbit coupled BEC [37–39], whose double-well band dispersion possesses two band minima at different momentum states, in analogy to real space Josephson junctions. The incorporation of a weak optical lattice induces a coupling between BECs located at two band minima, leading to the experimental observation of the long-lived (> 100 ms) superfluid stripe ground state [36]. Starting from the stripe ground state, a supercurrent through the momentum space junction is induced by a sudden quench of the Raman detuning between two band minima, similar to applying a voltage in a superconducting Josephson junction. The detuning quench displaces the initial stripe state from the ground state for the final detuning parameter, leading to periodic spin-momentum oscillations observed in experiments that are Josephson oscillations.

We observe two types of Josephson oscillations: (i) Josephson plasma oscillations, which are characterized

by a small change in population and small phase differences between the two BECs, excited through a weak change of the system ground state; (ii) regular Josephson oscillations with a large population oscillation and a continuous increase (or decrease) of the phase difference, excited through a large change of the ground state. Our experimental results show good agreement with a theoretical model based on a two-mode approximation and numerical simulation based on the nonlinear Gross-Pitaevskii (GP) equation. The observed constant plateau of the plasma oscillation frequency in the weak lattice region showcases the important role of nonlinear interactions. Furthermore, we find that the observed Josephson plasma oscillation frequency corresponds to the zero quasimomentum gap of the Bogoliubov excitations in the superfluid stripe phase, which, in our system, represents the mass of a pseudo-Goldstone mode [40] emerging from explicit symmetry breaking (here, the weak optical lattice breaks spatial translational symmetry). Pseudo-Goldstone modes, first proposed in particle physics [41], have been a long-sought phenomenon in many different fields, and our Letter provides one direct experimental evidence for observing such an exotic mode.

Description of the system.—The experimental setup for the spin-orbit coupled BEC [42] has been described in our previous work [36]. Briefly, a ^{87}Rb BEC is confined in a cigar-shaped crossed optical dipole trap [Fig. 1(a)]. An external magnetic field applied along the x axis lifts the degeneracy among the three Zeeman states (m_F) in the $F = 1$ hyperfine manifold. A pair of 789 nm Raman beams intersecting at approximately 45° angles with the x axis couples the $|\uparrow\rangle \equiv |1,-1\rangle$ and $|\downarrow\rangle \equiv |1,0\rangle$ Zeeman split states [Fig. 1(b)], which generates spin-orbit coupling (SOC) in the x direction. The Raman coupling provides an effective momentum offset of $2\hbar k_R$ between these two pseudospin states. Because of the quadratic Zeeman splitting, the $|1,+1\rangle$ state is sufficiently decoupled and does not play a significant role [42]. Additionally, two 1064 nm laser beams copropagating with the Raman beams create a weak stationary optical lattice $V_L(x) = 2\hbar\Omega_L \sin^2(k_L x)$ along the x direction, which provides a $2\hbar k_L$ momentum kick while keeping the spin unchanged. Additional experimental details involving the atomic states and energy scales are provided in [42].

The dynamics of the system can be described by the one-dimensional GP equation

$$i\partial_t \psi = [H_0 + g|\psi(x,t)|^2]\psi, \tag{1}$$

where $\psi = (\psi_\uparrow, \psi_\downarrow)^T$ is the two-component spinor wave function with the normalization to the total number of atoms $N = \int |\psi|^2 dx$, g is the density interaction strength, and $H_0 = H_{\mathrm{SOC}} + V_L(x)$ is the single-particle Hamiltonian with

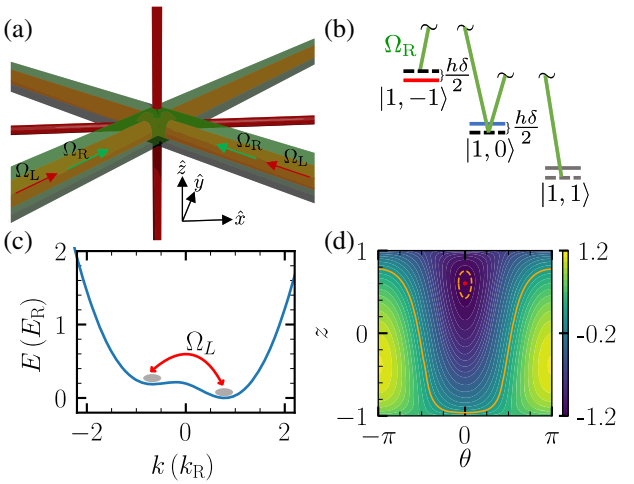

FIG. 1. Illustration of the experimental setup and the momentum space Josephson effect. (a) A crossed optical dipole trap (red) with two Raman laser beams (green) collinear with two optical lattice beams (red) intersecting at the BEC position in the center. (b) Two-photon Raman transitions within the $F = 1$ hyperfine manifold of ^{87}Rb. (c) Band structure of H_{SOC} for $\hbar\Omega_R = 2.7E_R$ and $\delta = 2\pi \times 500$ Hz. (d) Phase space diagram demonstrating Josephson dynamics for $\hbar\Omega_L = 0.5E_R$ and $gn = 0.25E_R$.

$$H_{\mathrm{SOC}} = (i\partial_x + \sigma_z)^2 - \frac{\delta}{2}\sigma_z + \frac{\Omega_R}{2}\sigma_x. \tag{2}$$

Here, Ω_R is the Raman coupling strength, δ is the detuning of the two-photon Raman transition, and $\hbar k_R$ and $E_R = (\hbar^2 k_R^2/2m) = h \times 1.96$ kHz are the momentum and energy units, respectively.

Figure 1(c) shows the momentum space double-well band dispersion of H_{SOC}. In the experiment, the period of the optical lattice is set such that $2\hbar k_L$ equals the separation between the two spin-orbit band minima [36]. The optical lattice leads to the hopping between the BECs at the two band minima, in analogy to the tunneling between two superconductors separated by an insulating barrier in a Josephson junction. While the optical lattice produces multiple off-resonance couplings in addition, the momentum space Josephson junction can be more intuitively understood using a two-mode approximation, i.e., considering only two BEC modes at two band minima with $\psi = (\phi_l \chi_l e^{-ik_L x} + \phi_r \chi_r e^{ik_L x}) e^{ik_b x}$, where χ_j are the spinor wave function at two band minima, $\phi_j(t)$ are the mode population coefficients, and k_b is the bias momentum induced by the detuning δ. This model also neglects modes in the excited band. Denoting $\phi_j = \sqrt{n_j} e^{i\theta_j}$, the GP equation can be projected as

$$\begin{aligned} \partial_\tau z &= -\sqrt{1-z^2}\sin\theta, \\ \partial_\tau \theta &= \Lambda z + \frac{z}{\sqrt{1-z^2}}\cos\theta - \Delta E \end{aligned} \tag{3}$$

in terms of the phase difference $\theta = \theta_l - \theta_r$ and relative population difference $z = (n_r - n_l)/n$, where $n = n_l + n_r$ is taken as a constant by neglecting populations in other modes. $\tau = 2Kt$, where $K = (\Omega_L/2)\chi_l^*\chi_r$ describes the hopping between the two modes (K is chosen to be real without loss of generality). $\Lambda = -Un/(2K)$, where $U = g|\chi_l^*\chi_r|^2$ represents the interaction strength of the BECs with two modes. $\Delta E = (E_l - E_r)/(2K)$, with $E_j = \int dx \chi_j^* H_0 \chi_j + (g+U)n$, is the energy difference between the two modes. Equation (3) describes a Bose Josephson junction governed by the effective Hamiltonian $H_{\text{eff}} = (\Lambda/2)z^2 - \sqrt{1-z^2}\cos\theta - \Delta E z$ [15].

A typical phase space diagram is shown in Fig. 1(d) to illustrate the momentum space Josephson dynamics. The red fixed point (z_0, θ_0) corresponds to the equilibrium ground state that can be obtained by finding the minima of H_{eff}. When the BEC is initially prepared away from (z_0, θ_0), (z, θ) oscillates following periodic orbits in phase space, corresponding to Josephson oscillation between BECs at two band minima. There are two different types of oscillating behavior: (i) When the BEC is initially prepared not far from the fixed point, θ changes only within a small range for the closed periodic orbits, representing Josephson plasma oscillation shown as the orange dashed line; (ii) when the BEC is far from the fixed point, θ increases (or decreases) continuously through $[0, 2\pi]$, corresponding to regular Josephson oscillation shown as the orange solid line [15].

Observation of Josephson oscillation.—In our experiments, we observe momentum space Josephson dynamics after a sudden quench of the Raman detuning from an initial value δ_i to a final value δ_f, in analogy to the voltage-driven ac Josephson effect. After the quench, the initially prepared superstripe state at δ_i is no longer the ground state at δ_f. The BEC will then evolve under the two-mode approximation along a periodic orbit around the fixed point for δ_f, demonstrating the Josephson oscillation. The starting point of the experiment is the preparation of a superfluid stripe state through Raman and optical lattice dressing of the BEC [36]. SOC is generated by adiabatically ramping on the Raman beams such that the Raman coupling strength $\hbar\Omega_R$ increases from 0 to $2.7E_R$ in 50 ms. During this time, the Raman coupling is far detuned [typically, $\delta = 2\pi \times (5.5\ \text{kHz} \pm 100\ \text{Hz})$] from the resonance. The optical lattice beams are then adiabatically applied, increasing $\hbar\Omega_L$ from 0 to the desired strength in 50 ms. Following that, δ is linearly decreased to a desired value δ_i in 50 ms. This adiabatic process prepares the BEC in the superfluid stripe ground state for δ_i.

In the case of a Josephson plasma oscillation, (z, θ) oscillates along a small closed orbit around (z_0, θ_0) in phase space. We choose a fixed $\delta_f = 2\pi \times 500$ Hz and different $\delta_i = 2\pi \times (500\ \text{Hz} + Q)$ for different $\hbar\Omega_L \in \{0.2, 0.4, \ldots, 1.4\}E_R$. Proper reasoning for choosing a finite value of the final Raman detuning (δ_f) can be found in [42]. Suitable values of the quench frequency Q are chosen such that spin oscillations are still observable, but the initial (z_i, θ_i) do not deviate significantly from (z_0, θ_0), leading to plasma oscillation. After the sudden quench $\delta_i \to \delta_f$, we let the BEC evolve for a time t in the presence of the Raman and optical lattice couplings. Subsequently, the Raman and lattice beams are switched off; the BEC is released from the crossed optical dipole trap, and a 17.5-ms-long time of flight (TOF), along with a briefly applied Stern-Gerlach field, resolves the BEC into different bare spin-momentum eigenstates. In the absorption images of the BEC, the two spin states are separated vertically, and, for each spin state, the momentum components are resolved horizontally [36] (Fig. 2). We measure the total spin polarization $\langle\sigma_z\rangle = (N_\uparrow - N_\downarrow)/(N_\uparrow + N_\downarrow)$ at each time t, where $N_\uparrow$ and $N_\downarrow$ are the total number of atoms in spin $|\uparrow\rangle$ and $|\downarrow\rangle$, respectively. Notice that $\langle\sigma_z\rangle = \sum_j (n_j/n)\langle\chi_j|\sigma_z|\chi_j\rangle$, which can be written as $\langle\sigma_z\rangle = a + bz$ under the two-mode approximation, with $2a = \langle\chi_l|\sigma_z|\chi_l\rangle + \langle\chi_r|\sigma_z|\chi_r\rangle$ and $2b = \langle\chi_r|\sigma_z|\chi_r\rangle - \langle\chi_l|\sigma_z|\chi_l\rangle$. Therefore, the spin polarization oscillates with the same frequency as the Josephson oscillation. For the parameters in Fig. 3, we have $a = 0.0493$ and $b = 0.732$ [42].

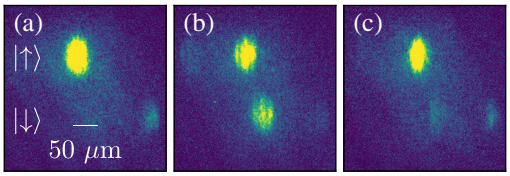

FIG. 2. Spin-momentum oscillation in a double-well SOC BEC. (a)–(c) Absorption images for $\hbar\Omega_L = 0.4E_R$ after an evolution time of $t = 0.15$, 1.05, and 1.65 ms.

Figures 3(a)–3(c) show the oscillations of $\langle\sigma_z\rangle$ during the postquench time t, measured for three different lattice coupling strengths. The corresponding quench, optical lattice coupling strength, and the spin-polarization oscillation frequency $(Q, \hbar\Omega_L, \Delta)$ for the three cases are (a) [1.3 kHz, $0.2E_R$, $(0.287 \pm 0.007)E_R$], (b) [200 Hz, $1.0E_R$, $(0.530 \pm 0.016)E_R$], and (c) [400 Hz, $1.4E_R$, $(0.734 \pm 0.039)E_R$], where the errors in oscillation frequencies represent the standard errors in Δ obtained from the sinusoidal fitting of the corresponding dataset. The experimentally observed time evolution of $\langle\sigma_z\rangle$ agrees reasonably well with the numerical results from directly simulating the quench dynamics using the GP Eq. (1) [42]. In Fig. 3(d), we show experimentally measured Josephson plasma oscillation frequencies with respect to $\hbar\Omega_L$ and their comparison with several theoretical models and numerical calculations for the interaction strength $gn = 0.25E_R$. The constant Josephson plasma frequency for small values of $\hbar\Omega_L$ indicates a nonlinear interaction in the system, as evidenced by the comparison to the

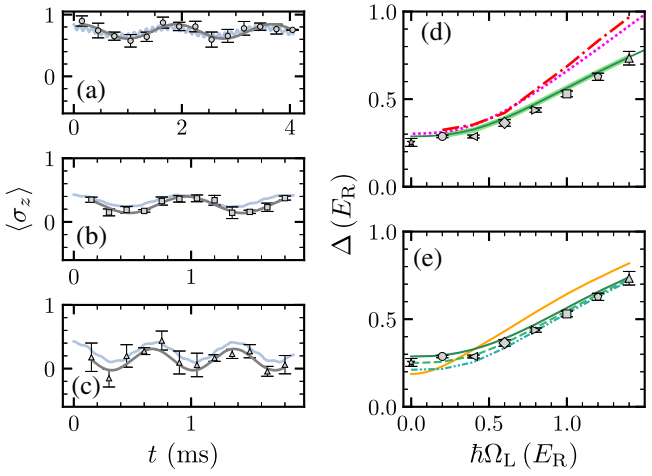

FIG. 3. Josephson plasma oscillation after Raman detuning quench. (a)–(c) Oscillation of the spin polarization for three different lattice coupling strengths (see the main text for parameters). The solid black (light blue) curves represent the sinusoidal fitting of the experimental data (GP simulation results), while the symbols with error bars are the experimental data points. (d) Comparison between the observed Δ (symbols with error bars) and predicted Δ obtained from analyzing the Bogoliubov spectrum (solid green line), quench dynamics using the GP equation (thick solid green line), perturbation analysis of the two-mode Josephson model (densely dotted magenta line), and the quench dynamics of Josephson model (dash-dotted red line). (e) Comparison of the Bogoliubov spectrum analysis for $gn = 0.25E_R$ and final Raman detuning $\delta_f = 2\pi \times 500$ (green solid line), 400 (green dashed line), and 300 Hz (green densely dash-dot-dotted line) with the experimental data points for $\delta_f = 2\pi \times 500$ Hz. The solid orange line represents the calculated variation of Δ with $\hbar\Omega_L$ for $\delta_f = 2\pi \times 500$ Hz and $gn = 0$ (noninteracting case). The distinct markers represent the oscillation frequency experimentally obtained for the corresponding $\hbar\Omega_L$ from the time-dependent $\langle\sigma_z\rangle$ plots in (a)–(c) and similar additional plots in [42]. The star markers at $\hbar\Omega_L = 0$ in (d) and (e) are obtained from Bragg spectroscopic measurements on a SOC BEC [42].

noninteracting case [Fig. 3(e)]. Additionally, Fig. 3(e) shows the dependence of the plasma oscillation frequencies (Δ) on the Raman detuning (δ), which is an experimental parameter [42]. The different theoretical models and numerical calculations are described below. (i) Numerical simulations of GP Eq. (1), which agree well with the experimental data for all $\hbar\Omega_L$. (ii) Numerical simulations of the effective dynamics (3) from the two-mode approximation. In such detuning quench-driven dynamics, we have $\theta_i = 0$, as seen from the fixed point position in the phase space diagram. Starting from the initial z_i for δ_i, we numerically integrate Eq. (3) and determine the oscillation frequency. (iii) Perturbation analysis of the two-mode dynamics. For the case of a small quench, we can treat the dynamics around the fixed point $(z_0, \theta_0 = 0)$ for δ_f as a perturbation, i.e., $z = z_0 + \delta z$, $\theta = \delta\theta$, yielding

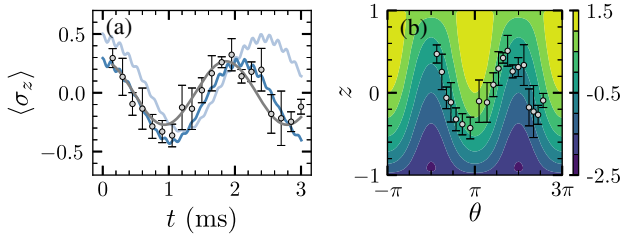

FIG. 4. Regular Josephson oscillation after Raman detuning quench. (a) Oscillation of the spin polarization. The solid black (light blue) curve represents a sinusoidal fit of the experimental data (GP simulation results). The dark blue curve represents the GP simulation results for a Raman detuning quench of $\delta_i = 2\pi \times 30$ Hz to $\delta_f = -2\pi \times 570$ Hz. (b) $z - \theta$ phase space diagram for $\hbar\Omega_L = 0.2E_R$ and $gn = 0.25E_R$ along with the experimental data. The points shown are obtained by calculating θ theoretically for the experimentally measured z values according to $\langle\sigma_z\rangle = a + bz$ [42]. Contour lines correspond to orbits with different energy.

$$\partial_\tau \delta z = -\sqrt{1 - z_0^2}\,\delta\theta,$$
$$\partial_\tau \delta\theta = \left[\Lambda + (1 - z_0^2)^{-3/2}\right]\delta z, \tag{4}$$

with initial conditions $\delta z(0) = z_i - z_0$ and $\delta\theta(0) = \theta_i - \theta_0 = 0$. Therefore, the oscillation frequency $\Delta = 2K[\sqrt{1 - z_0^2}\Lambda + (1 - z_0^2)^{-1}]^{1/2}$. Note that the initial imbalance z_0 also depends on the lattice strength, and, as $\hbar\Omega_L \to 0$, one has $z_0 \to -1$ and $K \to 0$, leading to a finite Δ. A plot of z_0 with respect to $\hbar\Omega_L$ is shown in [42]. The analytic expression agrees well with the numerical results in (ii) but deviates from the experimental results and GP simulation significantly in the large $\hbar\Omega_L$ regime, where higher-energy modes in the SOC band are coupled by the optical lattice, leading to the failure of the two-mode approximation. (iv) The zero quasimomentum gap of the Bogoliubov excitation spectrum. The sudden quench of the detuning leads to collective Bogoliubov quasiparticle excitations of the BEC located at quasimomentum $q = 0$ due to the lack of momentum transfer. When the quench is weak, only the lowest quasiparticle band is excited. Therefore, the plasma oscillation frequency can be determined from the lowest Bogoliubov band gap. Details of this analysis and its connection with the pseudo-Goldstone mode are discussed in the next section.

While the phase varies only within a small range for a Josephson plasma oscillation, it can continuously vary through $[0, 2\pi]$ for a regular Josephson oscillation. We access this regime by choosing a larger quench $\delta_i = 2\pi \times 100$ Hz and $\delta_f = -2\pi \times 500$ Hz with $\hbar\Omega_L = 0.2E_R$ so that the initial z_i is far from the fixed point z_0. Figure 4(a) shows the spin-polarization oscillation as a function of the post-quench time t, demonstrating a large amplitude of oscillation with a change of sign in $\langle\sigma_z\rangle$ and an oscillation frequency of $(0.275 \pm 0.011)E_R$. In Fig. 4(b), we show a

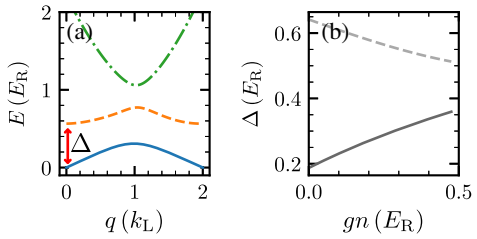

FIG. 5. (a) Bogoliubov spectrum of H_0 for $\hbar\Omega_R = 2.7E_R$, $\hbar\Omega_L = 1E_R$, $\delta = 2\pi \times 500$ Hz, and $gn = 0.25E_R$. (b) Dependence of zero quasimomentum ($q = 0$) band gap (Δ) on gn for $\hbar\Omega_L = 0$ (solid line) and $\hbar\Omega_L = 1E_R$ (dashed line).

contour plot for the variation of the phase θ with z. The data points in Fig. 4(b) are obtained by calculating θ theoretically for the experimentally measured z values according to $\langle\sigma_z\rangle = a + bz$ [42]. The error in z represents the standard error calculated from the standard deviation in $\langle\sigma_z\rangle$. Figure 4(a) shows the regular Josephson oscillation in momentum space, with a suboptimal agreement between the theory and experiment. The dark blue curve shows the numerical GP simulation results for a Raman detuning (δ) shift of 70 Hz, which is within the range of ± 100 Hz uncertainty and demonstrates a better agreement.

Connection with Bogoliubov spectrum and pseudo-Goldstone mode.—As discussed in (iv), a small sudden Raman detuning quench generates collective excitations of the BEC from the ground band to the first excited band. The modified band structure with the incorporation of the optical lattice and mean field interaction is shown in Fig. 5(a). Without the optical lattice and in the absence of a Raman detuning δ, the system has translational symmetry, and the interaction leads to two gapless Goldstone modes for the stripe phase [48]. The weak optical lattice breaks the translational symmetry explicitly, causing one Goldstone mode to become gapped at zero quasimomentum $q = 0$. This mode is then referred to as a pseudo-Goldstone mode, which is highly relevant in the context of particle and condensed matter physics [40]. The dependence of this pseudo-Goldstone gap on the mean-field interaction is shown in Fig. 5(b). The comparison between the experimentally measured Josephson plasma oscillation frequency and the Bogoliubov excitation gap is shown in Figs. 3(d) and 3(e). We see that the Bogoliubov gap agrees well with the experimental measurement as well as the GP simulation. Clearly, mean-field interactions play an important role in the zero quasimomentum band gap [42]. As expected, the Bogoliubov gaps agree with those obtained from two-mode Josephson dynamics in shallow lattice regimes. The gap deviates significantly in deep lattice regimes due to the coupling with higher-momentum modes.

The connection between the Josephson oscillation frequency and the pseudo-Goldstone gap can be understood as follows. Consider a small deviation of the wave function away from the ground state

$$\psi = [(\phi_l^0 + \delta\phi_l)\chi_l e^{-ik_L x} + (\phi_r^0 + \delta\phi_r)\chi_r e^{ik_L x}]e^{ik_b x}, \quad (5)$$

that is, Bogoliubov excitations with the two-mode approximation. $\delta\phi_l$ and $\delta\phi_r$ can be obtained by solving their corresponding Bogoliubov equation [42,49]. Comparing with Eq. (4), we find $\delta z = -2\sum_j \mathrm{Re}[(-1)^j \delta\phi_j^* \phi_j^0]$ and $\delta\theta = -\sum_j \mathrm{Im}[(-1)^j \delta\phi_j/\phi_j^0]$. By examining the two lowest modes at $q = 0$, one finds that the gapped (gapless) one gives rise to nonvanishing (vanishing) δz and $\delta\theta$. Therefore, the Josephson plasma oscillation frequency is just the zero quasimomentum Bogoliubov roton gap.

The symmetry-breaking origin of the pseudo-Goldstone mode can also be intuitively understood in the effective two-mode dynamics. Without the coupling K (induced by the optical lattice), Eq. (3) has a $U_s(1) \times U_a(1)$ symmetry, where $U_s(1)$ corresponds to the simultaneous rotation of two modes and $U_a(1)$ represents equal but opposite phase rotation of two modes. The spontaneous symmetry breaking leads to two uncoupled gapless modes (i.e., the Goldstone modes). The introduction of a coupling $K \neq 0$ breaks the symmetry $U_a(1)$ and reduces the system symmetry to $U_s(1)$. This $U_s(1)$ symmetry is spontaneously broken, and the attendant Goldstone boson is absorbed and removed from the spectra via the Higgs mechanism [43]. Only the second Goldstone boson corresponding to symmetry $U_a(1)$ appears. The parameter K is the soft breaking parameter of the symmetry $U_a(1)$, and the corresponding excitations become pseudo-Goldstone bosons.

Conclusion and discussion.—Our Letter offers a new experimental platform for designing exotic quantum matter and engineering quantum simulators utilizing momentum states as a synthetic degree of freedom. For instance, applying Bragg scattering to the superfluid stripe ground state, one can measure the Bogoliubov excitation spectrum at finite quasimomentum, leading to the full characterization of the long-sought pseudo-Goldstone mode. Because of the spin-momentum coupling, the density interaction in the superfluid stripe phase could induce strong spin squeezing, which may be realized in our platform and used for quantum sensing. Applying small but periodic modulations of the Raman detuning can lead to the observation of a Shapiro resonance in the momentum space Josephson junction. These novel quantum phenomena enabled by the momentum space Josephson junction could potentially be useful for quantum technologies.

A. M., C. S., M. K. H. O., S. M., and P. E. acknowledge funding from National Science Foundation (NSF) through Grant No. PHY-1912540. P. E. also acknowledges support through the Ralph G. Yount Distinguished Professorship at WSU. We acknowledge experimental support from Ethan Crowell during the initial stage of this project. C. Z. is supported by Air Force Office of Scientific Research (FA9550-20-1-0220) and NSF (PHY-2409943, OMR-2228725, and ECC-2411394). X. L. acknowledges support

from the Innovation Program for Quantum Science and Technology (Grant No. 2021ZD0301200), the National Natural Science Foundation of China (No. 12275203), and the USTC start-up funding.

*These authors contributed equally to this work.
†chuanwei.zhang@wustl.edu
‡engels@wsu.edu

[1] B. Josephson, Possible new effects in superconductive tunnelling, Phys. Lett. **1**, 251 (1962).
[2] B. D. Josephson, The discovery of tunnelling supercurrents, Rev. Mod. Phys. **46**, 251 (1974).
[3] P. W. Anderson and J. M. Rowell, Probable observation of the Josephson superconducting tunneling effect, Phys. Rev. Lett. **10**, 230 (1963).
[4] S. Backhaus, S. V. Pereverzev, A. Loshak, J. C. Davis, and R. E. Packard, Direct measurement of the current-phase relation of a superfluid ^{3}He-B weak link, Science **278**, 1435 (1997).
[5] J. C. Wheatley, Experimental properties of superfluid ^{3}He, Rev. Mod. Phys. **47**, 415 (1975).
[6] A. J. Leggett, A theoretical description of the new phases of liquid ^{3}He, Rev. Mod. Phys. **47**, 331 (1975).
[7] K. Sukhatme, Y. Mukharsky, T. Chui, and D. Pearson, Observation of the ideal Josephson effect in superfluid ^{4}He, Nature (London) **411**, 280 (2001).
[8] E. Hoskinson, R. Packard, and T. M. Haard, Quantum whistling in superfluid helium-4, Nature (London) **433**, 376 (2005).
[9] M. Abbarchi, A. Amo, V. Sala, D. Solnyshkov, H. Flayac, L. Ferrier, I. Sagnes, E. Galopin, A. Lemaître, G. Malpuech *et al.*, Macroscopic quantum self-trapping and Josephson oscillations of exciton polaritons, Nat. Phys. **9**, 275 (2013).
[10] M. Albiez, R. Gati, J. Fölling, S. Hunsmann, M. Cristiani, and M. K. Oberthaler, Direct observation of tunneling and nonlinear self-trapping in a single bosonic Josephson junction, Phys. Rev. Lett. **95**, 010402 (2005).
[11] S. Levy, E. Lahoud, I. Shomroni, and J. Steinhauer, The ac and dc Josephson effects in a Bose-Einstein condensate, Nature (London) **449**, 579 (2007).
[12] F. Dalfovo, L. Pitaevskii, and S. Stringari, Order parameter at the boundary of a trapped Bose gas, Phys. Rev. A **54**, 4213 (1996).
[13] F. Dalfovo, S. Giorgini, L. P. Pitaevskii, and S. Stringari, Theory of Bose-Einstein condensation in trapped gases, Rev. Mod. Phys. **71**, 463 (1999).
[14] M. R. Andrews, C. G. Townsend, H.-J. Miesner, D. S. Durfee, D. M. Kurn, and W. Ketterle, Observation of interference between two Bose condensates, Science **275**, 637 (1997).
[15] A. Smerzi, S. Fantoni, S. Giovanazzi, and S. R. Shenoy, Quantum coherent atomic tunneling between two trapped Bose-Einstein condensates, Phys. Rev. Lett. **79**, 4950 (1997).
[16] P. Öhberg and S. Stenholm, Internal Josephson effect in trapped double condensates, Phys. Rev. A **59**, 3890 (1999).
[17] J. Williams, R. Walser, J. Cooper, E. Cornell, and M. Holland, Nonlinear Josephson-type oscillations of a driven, two-component Bose-Einstein condensate, Phys. Rev. A **59**, R31 (1999).
[18] S. Raghavan, A. Smerzi, S. Fantoni, and S. R. Shenoy, Coherent oscillations between two weakly coupled Bose-Einstein condensates: Josephson effects, π oscillations, and macroscopic quantum self-trapping, Phys. Rev. A **59**, 620 (1999).
[19] F. S. Cataliotti, S. Burger, C. Fort, P. Maddaloni, F. Minardi, A. Trombettoni, A. Smerzi, and M. Inguscio, Josephson junction arrays with Bose-Einstein condensates, Science **293**, 843 (2001).
[20] T. Zibold, E. Nicklas, C. Gross, and M. K. Oberthaler, Classical bifurcation at the transition from Rabi to Josephson dynamics, Phys. Rev. Lett. **105**, 204101 (2010).
[21] J. M. Kreula, G. Valtolina, and P. Törmä, Spin-asymmetric Josephson plasma oscillations, Phys. Rev. A **95**, 013634 (2017).
[22] G. Spagnolli, G. Semeghini, L. Masi, G. Ferioli, A. Trenkwalder, S. Coop, M. Landini, L. Pezzè, G. Modugno, M. Inguscio, A. Smerzi, and M. Fattori, Crossing over from attractive to repulsive interactions in a tunneling bosonic Josephson junction, Phys. Rev. Lett. **118**, 230403 (2017).
[23] A. Burchianti, C. Fort, and M. Modugno, Josephson plasma oscillations and the Gross-Pitaevskii equation: Bogoliubov approach versus two-mode model, Phys. Rev. A **95**, 023627 (2017).
[24] A. Burchianti, F. Scazza, A. Amico, G. Valtolina, J. A. Seman, C. Fort, M. Zaccanti, M. Inguscio, and G. Roati, Connecting dissipation and phase slips in a Josephson junction between fermionic superfluids, Phys. Rev. Lett. **120**, 025302 (2018).
[25] G. Valtolina, A. Burchianti, A. Amico, E. Neri, K. Xhani, J. A. Seman, A. Trombettoni, A. Smerzi, M. Zaccanti, M. Inguscio, and G. Roati, Josephson effect in fermionic superfluids across the BEC-BCS crossover, Science **350**, 1505 (2015).
[26] N. Luick, L. Sobirey, M. Bohlen, V. P. Singh, L. Mathey, T. Lompe, and H. Moritz, An ideal Josephson junction in an ultracold two-dimensional Fermi gas, Science **369**, 89 (2020).
[27] Y. Makhlin, G. Schön, and A. Shnirman, Quantum-state engineering with Josephson-junction devices, Rev. Mod. Phys. **73**, 357 (2001).
[28] C. Ryu, P. W. Blackburn, A. A. Blinova, and M. G. Boshier, Experimental realization of Josephson junctions for an atom SQUID, Phys. Rev. Lett. **111**, 205301 (2013).
[29] J. M. Martinis, S. Nam, J. Aumentado, and C. Urbina, Rabi oscillations in a large Josephson-junction qubit, Phys. Rev. Lett. **89**, 117901 (2002).
[30] O. Astafiev, Y. A. Pashkin, Y. Nakamura, T. Yamamoto, and J. S. Tsai, Temperature square dependence of the low frequency $1/f$ charge noise in the Josephson junction qubits, Phys. Rev. Lett. **96**, 137001 (2006).
[31] J. M. Martinis, M. Ansmann, and J. Aumentado, Energy decay in superconducting Josephson-junction qubits from nonequilibrium quasiparticle excitations, Phys. Rev. Lett. **103**, 097002 (2009).
[32] H. Paik, D. I. Schuster, L. S. Bishop, G. Kirchmair, G. Catelani, A. P. Sears, B. R. Johnson, M. J. Reagor, L. Frunzio, L. I. Glazman, S. M. Girvin, M. H. Devoret, and

R. J. Schoelkopf, Observation of high coherence in Josephson junction qubits measured in a three-dimensional circuit QED architecture, Phys. Rev. Lett. **107**, 240501 (2011).

[33] J. Hou, X.-W. Luo, K. Sun, T. Bersano, V. Gokhroo, S. Mossman, P. Engels, and C. Zhang, Momentum-space Josephson effects, Phys. Rev. Lett. **120**, 120401 (2018).

[34] F. A. An, E. J. Meier, J. Ang'ong'a, and B. Gadway, Correlated dynamics in a synthetic lattice of momentum states, Phys. Rev. Lett. **120**, 040407 (2018).

[35] F. A. An, B. Sundar, J. Hou, X.-W. Luo, E. J. Meier, C. Zhang, K. R. A. Hazzard, and B. Gadway, Nonlinear dynamics in a synthetic momentum-state lattice, Phys. Rev. Lett. **127**, 130401 (2021).

[36] T. M. Bersano, J. Hou, S. Mossman, V. Gokhroo, X.-W. Luo, K. Sun, C. Zhang, and P. Engels, Experimental realization of a long-lived striped Bose-Einstein condensate induced by momentum-space hopping, Phys. Rev. A **99**, 051602(R) (2019).

[37] Y.-J. Lin, K. Jiménez-García, and I. B. Spielman, Spin-orbit-coupled Bose-Einstein condensates, Nature (London) **471**, 83 (2011).

[38] K. Jiménez-García, L. J. LeBlanc, R. A. Williams, M. C. Beeler, C. Qu, M. Gong, C. Zhang, and I. B. Spielman, Tunable spin-orbit coupling via strong driving in ultracold-atom systems, Phys. Rev. Lett. **114**, 125301 (2015).

[39] Y. Zhang, M. E. Mossman, T. Busch, P. Engels, and C. Zhang, Properties of spin-orbit-coupled Bose-Einstein condensates, Front. Phys. **11**, 118103 (2016).

[40] C. Burgess, Goldstone and pseudo-goldstone bosons in nuclear, particle and condensed-matter physics, Phys. Rep. **330**, 193 (2000).

[41] S. Weinberg, Approximate symmetries and pseudo-goldstone bosons, Phys. Rev. Lett. **29**, 1698 (1972).

[42] See Supplemental Material at http://link.aps.org/supplemental/10.1103/PhysRevLett.132.233403 for more theoretical details about the model, Josephson GP dynamics, and the relation with the Bogoliubov spectrum, as well as some experimental details about the parameters and Bragg spectrum, which includes Refs. [36,37,43–47].

[43] F. P. Esposito, L.-P. Guay, R. B. MacKenzie, M. B. Paranjape, and L. C. R. Wijewardhana, Field theoretic description of the abelian and non-abelian Josephson effect, Phys. Rev. Lett. **98**, 241602 (2007).

[44] C. Wang, C. Gao, C.-M. Jian, and H. Zhai, Spin-orbit coupled spinor Bose-Einstein condensates, Phys. Rev. Lett. **105**, 160403 (2010).

[45] T.-L. Ho and S. Zhang, Bose-Einstein condensates with spin-orbit interaction, Phys. Rev. Lett. **107**, 150403 (2011).

[46] Y. Li, L. P. Pitaevskii, and S. Stringari, Quantum tricriticality and phase transitions in spin-orbit coupled Bose-Einstein condensates, Phys. Rev. Lett. **108**, 225301 (2012).

[47] M. A. Khamehchi, Y. Zhang, C. Hamner, T. Busch, and P. Engels, Measurement of collective excitations in a spin-orbit-coupled Bose-Einstein condensate, Phys. Rev. A **90**, 063624 (2014).

[48] Y. Li, G. I. Martone, L. P. Pitaevskii, and S. Stringari, Superstripes and the excitation spectrum of a spin-orbit-coupled Bose-Einstein condensate, Phys. Rev. Lett. **110**, 235302 (2013).

[49] G.-Q. Li, X.-W. Luo, J. Hou, and C. Zhang, Pseudo-Goldstone excitations in a striped Bose-Einstein condensate, Phys. Rev. A **104**, 023311 (2021).